

Interplay of Electron-Phonon Interaction and Electron Correlation in High Temperature Superconductivity

Sumio Ishihara

Department of Physics, Tohoku University, Sendai 980-8578, Japan

Naoto Nagaosa

CREST, Department of Applied Physics, University of Tokyo, Tokyo 113-8656, Japan

and Correlated Electron Research Center, Agency of Industrial Science and Technology, Tsukuba, 305-0046, Japan
(March 20, 2018)

We study the electron-phonon interaction in the strongly correlated superconducting cuprates. Two types of the electron-phonon interactions are introduced in the $t - J$ model; the diagonal and off-diagonal interactions which modify the formation energy of the Zhang-Rice singlet and its transfer integral, respectively. The characteristic phonon-momentum (\vec{q}) and electron-momentum (\vec{k}) dependence resulted from the off-diagonal coupling can explain a variety of experiments. The vertex correction for the electron-phonon interaction is formulated in the SU(2) slave-boson theory by taking into account the collective modes in the superconducting ground states. It is shown that the vertex correction enhances the attractive potential for the d -wave paring mediated by phonon with $\vec{q} = (\pi(1 - \delta), 0)$ around $\delta \cong 0.3$ which corresponds to the half-breathing mode of the oxygen motion.

PACS numbers: 74.20.-z, 74.25.Kc, 74.20.Rp, 74.25.Ha

I. INTRODCUTION

It is widely accepted that the central issue in the high transition-temperature (T_c) superconducting (HTSC) cuprates is physics of the doped Mott insulator. The Mott-Hubbard (charge-transfer) insulating state with the antiferromagnetic long-range order in the parent compounds is well understood in strong Coulomb interaction between electrons. It is, then, well recognized that the electronic models with strong electron correlation provide a good starting point to reveal the electronic structure in doped Mott insulator. For example, one of the successful examples is the slave-boson mean-field theory in the two-dimensional $t - J$ model and its extensions to the gauge theory which can explain a wide range of unusual properties both in the normal and superconducting states; the phase diagram in hole concentration x and temperature T , paring symmetry, pseudogap and so on.¹⁻⁵

In spite of such successful results in the correlated electronic models, one shall have the questions that the electronic model alone is enough to explain essential physics in HTSC cuprates. Actually, since the early stage of the HTSC researches, a variety of experiments exhibit the lattice/phonon anomalies and the strong electron-lattice coupling which stimulate a number of theoretical works.⁶⁻¹¹ The finite isotope effects on T_c is one of the direct evidence of the phonon contribution to the paring interaction. The oxygen isotope coefficient α_O in $\text{La}_{2-x}\text{Sr}_x\text{CuO}_4$ (LSCO) around $x = 1/8$ exceeds 0.5 being greater than the expected value in the Bardeen-Cooper-Schrieffer (BCS) theory.¹² The isotope shift is also found in the magnetic penetration depth at zero temperature $\lambda(T = 0)$ (Ref. 13) which can not be understood within the standard BCS scenario. Anomalous phonon dispersion relation is directly observed by the

inelastic neutron scattering experiments. A strong softening and broadening of the highest longitudinal optic (LO) phonon with the oxygen in-plane Cu-O bond vibrations occurs along the $(q_x, 0)$ direction in LSCO.^{14,15} By doping of holes, the phonon energy ($\sim 85\text{meV}$) drastically reduces about 20% in the zone boundary, and is recovered in overdoped compound.¹⁶

A recently observed kink structure in high-resolution angular resolved photoemission spectroscopy (ARPES) spectra¹⁷⁻²⁰ triggers reexamination of the strong quasiparticle-phonon interaction in cuprates.²¹⁻²⁵ Here we summarize characteristic nature of this kink structure: (a) The kink structure is experimentally confirmed in a variety of the p-type cuprates: LSCO, $\text{Bi}_2\text{Sr}_2\text{CaCu}_2\text{O}_8$ (Bi2212), $\text{Bi}_2\text{Sr}_2\text{CuO}_6$ (Bi2201), $(\text{Ca}_{2-x}\text{Na}_x)\text{CuO}_2\text{Cl}_2$ (Na-CCOC), $\text{Tl}_2\text{Ba}_2\text{CuO}_6$ (Tl2201) and so on. On the other hand, this structure is weak in the n-type $\text{Nd}_{2-x}\text{Ce}_x\text{CuO}_4$ (NCCO). (b) The kink energy ω_{kink} about 70meV is almost universal. The quasi-particle velocity ratio above and below ω_{kink} , i.e. $R_v \equiv v(\omega > \omega_{\text{kink}})/v(\omega < \omega_{\text{kink}})$, is about 2 in optimal doped p-type cuprates and does not show the strong momentum dependence along the fermi surface. Below ω_{kink} , the quasi-particle width decreases rapidly. This is consistent with the rapid drop of the quasi-particle scattering rate deduced from the optical conductivity data.^{26,27} (c) The kink structure is seen far above T_c , and remarkable changes across T_c are not observed. (d) The quasi-particle velocity below the kink $v(\omega < \omega_{\text{kink}})$ along the nodal direction is almost universal in a wide range of HTSC.²⁸

This phenomena indicate the strong coupling between a bosonic excitation with energy ω_{kink} and the quasiparticles. It is suggested that there is a clear correlation between the quasiparticle velocity ratio across the

kink R_v , related to the electron-boson coupling strength, and the superconducting gap amplitude.²¹ A scenario based on the magnetic-resonance mode around 41meV as a bosonic excitation^{19,29,30} may be at a disadvantage; this excitation is only confirmed below T_c in $\text{YBa}_2\text{Cu}_3\text{O}_{6+x}$ (YBCO), Bi2212 and Tl2201. One of the plausible candidates for the origin of the kink structure is the optic phonon. The kink energy ω_{kink} is close to that of a LO phonon with the oxygen in-plane vibration whose anomalous softening and broadening are observed as described previously. This phonon scenario is strongly supported by the recent ARPES experiments for the isotope effects on the kink; in a Bi2212 sample with the O^{18} isotope, the kink energy ω_{kink} decreases about few meV from the standard O^{16} results. This result corresponds to the simultaneously observed lower shift of the LO phonon Raman spectra in the O^{18} sample.³¹

Here we mention another kink structure in the ARPES spectra in Bi2212.^{32–34} This is found near $(\pi, 0)$ and $(0, \pi)$ and, its kink energy is about 40meV measured from the Fermi energy. It has been claimed that this kink structure almost disappears above T_c , but recent more extensive study³⁴ found that it persists even above T_c . Therefore the c-axis buckling phonon, which has the appropriate energy of 40meV, is the most promising among the various candidates such as the magnetic resonance mode and the superconducting gap. However, we focus below the half-breathing mode which plays the major role in the nodal region.

In this paper, we study the electron-phonon interaction in the strongly correlated HTSC cuprates. The interactions between electron and phonon of the in-plane oxygen vibration mode are formulated in the $t - J$ model. There are two types of the couplings, i.e. the off-diagonal and diagonal interactions which modify the inter-site hopping of the Zhang-Rice singlet and its formation energy, respectively. We calculate the effective paring interaction, the quasiparticle renormalization factor, the ARPES, tunneling and optical spectra for the off-diagonal and diagonal couplings where the fermionic degree of freedom is assumed as a quasiparticle with the renormalized band energy. We show that the characteristic phonon-momentum (\vec{q}) and electron-momentum (\vec{k}) dependences resulted from the off-diagonal coupling are quite consistent with the experiments. This formulation and numerical results are presented in Sec. II. The vertex correction in the electron-phonon coupling is known to play a crucial role in correlated systems.^{40,41} This is studied, in the slave boson picture, by taking into account the fluctuations around the mean-field saddle-point solutions, that is, the d -wave paring order parameter Δ , the fermion hopping χ , the Lagrangian multipliers a and the bosonic field h . We formulate this vertex correction in the SU(2) slave-boson theory^{35–38} which respects an exact SU(2) gauge symmetry in the undoped case, and is expected to provide a better starting point than the U(1) theory in the underdoped region. The fluctuations are treated

as the collective modes in the ordered states,³⁹ and the electron-phonon interactions are corrected by the interaction between the collective modes and fermions. We show that the vertex correction enhances the effective interaction for the d -wave paring around $\vec{q} = (\pi(1 - \delta), 0)$ with $\delta \cong 0.3$ where the remarkable softening and broadening of the LO phonon are observed in the inelastic neutron scattering experiments. The roles of the vertex corrections are examined in Sec. III. Section IV is devoted to the summary and discussion. A part of the present theoretical works were briefly discussed in Ref. 21.

II. ELECTRON PHONON INTERACTION IN $T - J$ MODEL

A. Formulation of the Electron-Phonon Interaction

We will consider the electron-phonon interaction in the $t - J$ model.⁴²

$$\mathcal{H} = \sum_{i,\sigma} \varepsilon_i c_{i\sigma}^\dagger c_{i\sigma} - \sum_{\langle ij \rangle, \sigma} \left(t_{ij} c_{i\sigma}^\dagger c_{j\sigma} + H.c. \right) + \sum_{\langle ij \rangle} J_{ij} \vec{S}_i \cdot \vec{S}_j, \quad (1)$$

where $c_{i\sigma}$ is the annihilation operator of a hole at site i with spin σ , and is defined in the Hilbert space excluding the double occupancy. \vec{S}_i is the $S = 1/2$ spin operator at site i . The formation energy ε_i of the Zhang-Rice singlet at site i and its transfer integral t_{ij} between i and j are represented by the energy parameters in the original $p-d$ model as

$$\varepsilon_i = \frac{2t_{pd}^2}{\Delta_{pd}(i)}, \quad (2)$$

and

$$t_{ij} = t_{pd}^2 \frac{1}{2} \left\{ \frac{1}{\Delta_{pd}(i)} + \frac{1}{\Delta_{pd}(j)} \right\}, \quad (3)$$

respectively. The charge-transfer energy $\Delta_{pd}(i)$ is defined to be the energy difference of the p and d levels at site i : $\Delta_{pd}(i) = \varepsilon_p - \varepsilon_d(i)$ in the hole picture, and t_{pd} is the transfer integral between the nearest neighboring (NN) p and d orbitals. We assume that $U - \Delta_{pd}(i) \gg \Delta_{pd}(i)$.

Here, we introduce a motion of the oxygen ions along the Cu-O bond in the CuO₂ plane corresponding to the high-frequency optical phonon of our interest. The displacement of the negatively charged O ion along the Cu-O bond changes the electro-static Madelung potential acting on a Cu site and shifts the energy of the d level as $\varepsilon_d(i) = \varepsilon_{d0} + \delta\varepsilon_d(i)$ with

$$\delta\varepsilon_d(i) = gu(i), \quad (4)$$

within the linear electron-lattice coupling. $u(i)$ is a linear combination of the O displacements around the Cu site i (Fig. 1(a)) defined by

$$u(i) = u_x \left(i + \frac{a_x}{2} \right) - u_x \left(i - \frac{a_x}{2} \right) + u_y \left(i + \frac{a_y}{2} \right) - u_y \left(i - \frac{a_y}{2} \right), \quad (5)$$

where $u_l(i \pm \frac{a_l}{2})$ ($l = x, y$) indicates the displacement of the O ion at site $i \pm \frac{a_l}{2}$ along the direction l . The coupling constant g is positive, because the approach of the negatively charged O ion to the Cu site lowers the energy level for a hole. The O p level is not changed within the linear electron-lattice coupling, i.e. $\delta\varepsilon_p = 0$, because of symmetry. The modification of the charge-transfer energy is then given by $\Delta_{pd}(i) = \Delta_0 - gu(i)$. The O ion displacement also changes the transfer integral between p and d orbitals as

$$t_{pd} = t_0 \pm g_t u_l \left(i \pm \frac{a_l}{2} \right), \quad (6)$$

for a bond connecting a Cu site i and an O site $i \pm a_l/2$. The coupling constant g_t has an opposite sign of t_0 . As a result, the modulation of the formation energy of the Zhang-Rice singlet is given by

$$\varepsilon_i = \frac{2 \{t_0 + g_t u(i)\}^2}{\Delta_0 - gu(i)} \simeq \frac{2t_0^2}{\Delta_0} + g_{dia} u(i), \quad (7)$$

with

$$g_{dia} = \frac{2t_0^2}{\Delta_0} \left(\frac{g}{\Delta_0} + \frac{2g_t}{t_0} \right), \quad (8)$$

which is termed the diagonal electron-lattice coupling. We note that the two terms in the right-hand side have opposite sign with each other. In the similar way, the transfer integral of the Zhang-Rice singlet is modified as

$$t_{ij} = \frac{t_0^2}{\Delta_0} + g_{off} \{u(i) + u(j)\}, \quad (9)$$

with

$$g_{off} = g \frac{t_0^2}{2\Delta_0^2}, \quad (10)$$

termed the off-diagonal electron-lattice coupling. It is worth noting that the modulation of t_{pd} does not change t_{ij} . This is because, with a shift of a O ion at site $i + a_l/2$ along the positive l direction, a decrease in t_{pd} between site i and site $i + a_l/2$ is canceled out in the linear order by an increase in t_{pd} between $i + a_l$ and $i + a_l/2$. The electron-phonon interaction in the $t - J$ model is also brought about by the modulation of the superexchange interaction J_{ij} due to the O displacements. This type of electron-phonon coupling was first suggested to explain the two-magnon absorption spectra in undoped cuprates in Ref. 43. Here, we consider this electron-phonon coupling in the framework of the slave-boson mean-field theory. The detailed formulation based on the slave-boson theory is presented in Sec. III A. The constrained operator $c_{i\sigma}$ is represented, in this picture, by a product of the spinon (fermion) $f_{i\sigma}$ and holon (boson) h_i as

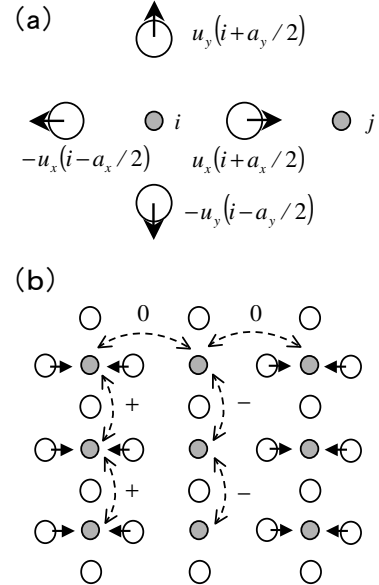


FIG. 1. (a) A linear combination of the O ion distortion $u(i) = u_x(i+a_x/2) + u_y(i+a_y/2) - u_x(i-a_x/2) - u_y(i-a_y/2)$. Open and filled circles indicate the O and Cu ions, respectively. (b) Schematic view of the half-breathing mode of the O vibration. +, - and 0 indicate signs of the modulation of the transfer integral t_{ij} between the NN Cu ions in this displacement.

$$c_{i\sigma} = f_{i\sigma} h_i^\dagger, \quad (11)$$

with the local constraint $\sum_\sigma f_{i\sigma}^\dagger f_{i\sigma} + h_i^\dagger h_i = 1$ in order to exclude the doubly occupied states. In the mean-field approximation, the J term in the $t - J$ model is rewritten by using the fermion hopping order-parameter χ_{ij} ($= \sum_\sigma f_{i\sigma}^\dagger f_{j\sigma}$) as

$$J_{ij} \vec{S}_i \cdot \vec{S}_j = -J_{ij} \chi_{ij}^\dagger \chi_{ij} \simeq -\frac{J_{ij}}{2} \left(\langle \chi_{ij}^\dagger \rangle \chi_{ij} + \chi_{ij}^\dagger \langle \chi_{ij} \rangle \right), \quad (12)$$

which is a similar form to the t term in Eq. (1). The fermion-lattice coupling through the modification of J is then reduced to the off-diagonal coupling as

$$J_{ij} = J_0 + g_J \{u(i) + u(j)\}, \quad (13)$$

where the coupling constant is given by

$$g_J = 6g \frac{t^4}{\Delta_0^4}. \quad (14)$$

In the standard slave-boson mean-field scheme, where the boson amplitude is taken to be \sqrt{x} in the ground state, the diagonal coupling constant g_{dia} and the off-diagonal one from the modulation of the transfer integral g_{off} are scaled by the factor x , and the coupling caused by the superexchange interaction g_J has a factor $1 - x$.

This implies that, in the Mott insulating limit of $x \rightarrow 0$, due to suppression of the charge fluctuation, the diagonal coupling becomes irrelevant, while the off-diagonal type survives because the modulation of J affects the spin channel. Even at nonzero (but small) x where the diagonal coupling becomes relevant, the vertex correction for the electron-phonon interaction, induced by the holon fluctuation, suppresses the diagonal coupling at the large momentum transfer.^{40,41} The vertex correction for the off-diagonal coupling is presented in Sec. III in more detail.

Consequently, the electron-phonon interaction Hamiltonian in the $t - J$ model is summarized as

$$\mathcal{H}_{el-ph} = \frac{1}{N} \sum_{\vec{k}, \vec{q}, \sigma} \sum_{\mu} g^{\mu}(\vec{k}, \vec{q}) \times f_{\vec{k} + \vec{q}\sigma}^{\dagger} f_{\vec{k}\sigma} \left(b_{\vec{q}}^{\mu} + b_{-\vec{q}}^{\mu\dagger} \right), \quad (15)$$

where $b_{\vec{q}}^{\mu}$ is the annihilation operator of phonon with momentum \vec{q} and the mode μ . We take the two independent modes $\mu = x$ and y where the O ions vibrate along the x and y directions, respectively. The electron-phonon coupling constant is given by a sum of the two-kind couplings

$$g^{\mu}(\vec{k}, \vec{q}) = g_{dia}^{\mu}(\vec{k}, \vec{q}) + g_{off}^{\mu}(\vec{k}, \vec{q}), \quad (16)$$

where

$$g_{dia}^{\mu}(\vec{k}, \vec{q}) = -2i g_{dia} \frac{1}{\sqrt{2MN\omega_{\vec{q}}^{\mu}}} \sin\left(\frac{q_{\mu}}{2}\right), \quad (17)$$

and

$$g_{off}^{\mu}(\vec{k}, \vec{q}) = -4i g_{off} \frac{1}{\sqrt{2MN\omega_{\vec{q}}^{\mu}}} \sin\left(\frac{q_{\mu}}{2}\right) \times \left\{ \cos k_x + \cos k_y + \cos(k_x + q_x) + \cos(k_y + q_y) \right\}, \quad (18)$$

with the oxygen mass M and the phonon frequency $\omega_{\vec{q}}^{\mu}$. The off-diagonal coupling constant g_{off} is redefined that g_{off} includes the contribution from g_J in Eq. (14). The diagonal-coupling constant $g_{dia}(\vec{k}, \vec{q})$ does not depend on the electron momentum \vec{k} as usual. Here, we note the characteristic electron-momentum \vec{k} and phonon-momentum \vec{q} dependences of the off-diagonal coupling $g_{off}^{\mu}(\vec{k}, \vec{q})$: (i) the fermion degree of freedom does not couple to the two-dimensional oxygen breathing mode, i.e. $g_{off}^{\mu}(\vec{k}, \vec{q} = (\pi, \pi)) = 0$. This is attributed to the fact that, for the breathing mode, $u(i) + u(j)$ in Eq. (9) becomes zero in all the NN Cu-Cu bonds. (ii) The coupling constant for the half-breathing mode where the O ions shift along l does not depend on the l component of the electron-momentum, e.g., $g_{off}^{\mu}(\vec{k}, \vec{q} = (\pi, 0))$ is independent of k_x . This is because this O ion displacement

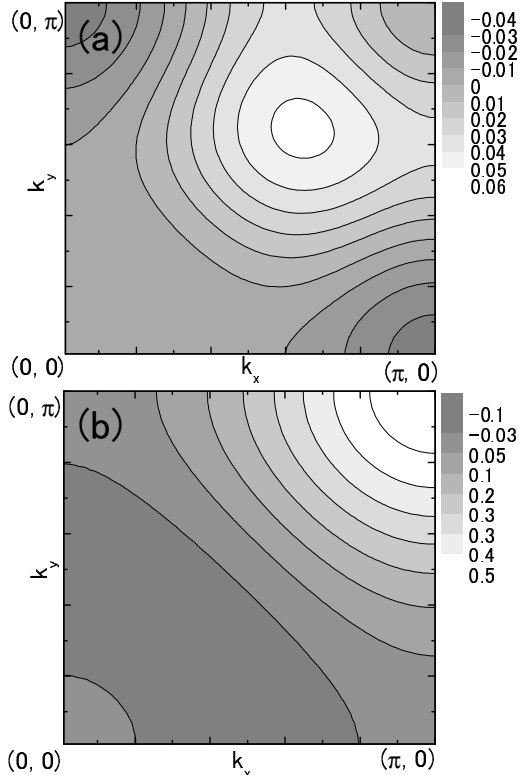


FIG. 2. Contour map of the effective paring interaction $F(\vec{q})$ in the off-diagonal coupling case (a), and in the diagonal coupling case (b). The energy gap is chosen to be $\phi_0 g_{off} = 0.035\text{eV}$ in (a), and $\phi_0 g_{dia} = 0.035\text{eV}$ in (b). Numerical data are plotted in a unit of eV. The phonon energy is chosen as $\omega_{ph} = 0.07\text{eV}$.

does not change t_{ij} along the direction l but change t_{ij} perpendicular to l . This characteristics of $g_{off}^{\mu}(\vec{k}, \vec{q})$ are schematically shown in Fig. 1 (b).

B. Physical consequences of the off-diagonal and diagonal electron-phonon couplings

We now turn to the numerical results for various physical quantities calculated from the electron-phonon interaction Hamiltonian introduced above. We pay attention, in particular, to the implications of the characteristic momentum dependence of the off-diagonal electron-phonon coupling. Then, we treat, in this section, an electron as a quasiparticle described by the renormalized energy band $\xi_{\vec{k}}$. This treatment corresponds to the mean-field approximation in the slave-boson theory where the Lagrangian is given in Eq. (35) in Sec. III A. In spite of the detailed form for the quasiparticle energy $\xi_{\vec{k}}$ in the slave-boson theory (see Eq. (36)), $\xi_{\vec{k}}$ is determined by the tight-bind fitting in Bi2212. The six tight-binding parameters are adopted by following the results in Refs. 29 and 44. The fluctuations from the mean-field saddle-points leading to

the vertex correction for the electron-phonon interaction are studied in the next section. The energy parameter values used in this section are given in a unit of eV. We assume that the phonon frequency ω_q^μ is independent of the mode μ and the momentum \vec{q} as $\omega_q^\mu = \omega_{ph}$, and choose $\omega_{ph} = 0.07$ eV. The electron-phonon coupling constants are scaled as $\tilde{g}_{dia(off)} = g_{dia(off)} / \sqrt{2MN\omega_q^\mu}$, and the damping constant is introduced in the calculation of spectra as $\gamma = 0.005$ eV.

We first show the effective paring interaction for the d -wave superconductivity due to the electron-phonon interaction. The momentum dependence of the effective electron-electron interaction is derived by integrating out the phonon degree of freedom in the electron-phonon interaction Hamiltonian. By using the second-order perturbational processes with respect to the electron-phonon coupling, the effective Hamiltonian is obtained as

$$\mathcal{H}_{eff} = -\frac{1}{N} \sum_{\vec{k}, \vec{k}', \vec{q}} \sum_{\sigma, \sigma', \mu} g^\mu(\vec{k}, \vec{q}) g^\mu(\vec{k}', -\vec{q}) \times \frac{\omega_q^\mu}{\omega_q^{\mu 2} - (\xi_{\vec{k}} - \xi_{\vec{k}+\vec{q}})^2} f_{\vec{k}+\vec{q}\sigma}^\dagger f_{\vec{k}\sigma} f_{\vec{k}'-\vec{q}\sigma'}^\dagger f_{\vec{k}'\sigma'}. \quad (19)$$

In the mean-field approximation according to the BCS theory, we obtain

$$\langle \mathcal{H}_{eff} \rangle = - \sum_{\vec{q}, \vec{k}, \mu} \frac{\omega_q^\mu}{\omega_q^{\mu 2} - (\xi_{\vec{k}} - \xi_{\vec{k}+\vec{q}})^2} |g^\mu(\vec{k}, \vec{q})|^2 \phi_{\vec{k}} \phi_{\vec{k}+\vec{q}} \simeq \sum_{\vec{q}, \mu} \frac{1}{\omega_q^\mu} F(\vec{q}), \quad (20)$$

where $|\xi_{\vec{k}} - \xi_{\vec{k}+\vec{q}}| \ll \omega_q^\mu$ is assumed. The paring order parameter is introduced as $\phi_{\vec{k}} = \langle f_{\vec{k}\uparrow} f_{\vec{k}\downarrow} \rangle$ and is parameterized as $\phi_{\vec{k}} = \phi_0(\cos k_x - \cos k_y)/2$ for the d -wave paring. $F(\vec{q})$ indicates the effective paring interaction between electrons contributed from the phonon with momentum \vec{q} . In Fig. 2(a), the contour map of $F(\vec{q})$ for the off-diagonal coupling is presented. The negative (positive) region corresponds to the attractive (repulsive) interaction for the d -wave paring. It is found that the phonon of the momentum $(q_x, 0)$ around $q_x = \pi$ strongly contributes to the d -wave paring. This phonon corresponds to the half-breathing mode of the O vibration where the anomalous softening of the dispersion relation is observed in the neutron experiments.^{14,15} The vanishing $F(\vec{q} = (\pi, \pi))$ indicates that the off-diagonal electron-lattice coupling does not disturb the attractive magnetic interaction dominated around (π, π) . This originates from the characteristic off-diagonal coupling that the breathing-mode of the O vibration does not couple to the fermion as pointed out above. The paring function $F(\vec{q})$ for the diagonal coupling is presented in Fig. 2(b) where the attractive interaction appears in the region of $q_x + q_y \lesssim \pi$. The most remarkable difference from the off-diagonal results is seen that the phonon around (π, π)

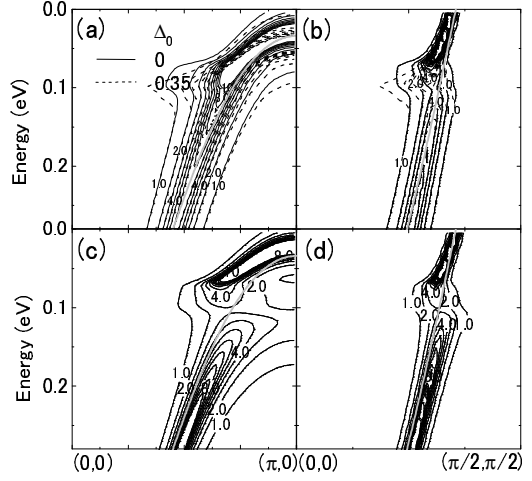


FIG. 3. Contour map of the fermion spectral density $A(\vec{k}, \omega)$ for the off-diagonal case (a) and (b) ($\tilde{g}_{off} = 0.03$ eV), and for the diagonal case (c) and (d) ($\tilde{g}_{dia} = 0.02$ eV). Solid lines indicate the spectra with $\Delta_0 = 0$ and dotted lines in (a) and (b) are for the spectra with $\Delta_0 = 0.035$ eV. Gray bold lines indicate the bare quasiparticle dispersion $\xi_{\vec{k}}$. The phonon energy is $\omega_{ph} = 0.07$ eV. Numerical data are plotted in a unit of eV^{-1} .

strongly suppresses the d -wave paring. That is, this diagonal coupling competes with the magnetic paring interaction.

The ARPES, tunneling and optical spectra are obtained in the Nambu-Eliashberg formulae. We calculate the self-energy for the 2×2 fermion Green's function:

$$\Sigma(\vec{k}, i\omega_n) = \sum_{\vec{q}, \omega_m, \mu} \tau_3 G_0(\vec{k} - \vec{q}, i\omega_n - i\omega_m) \tau_3 \times |g^\mu(\vec{k}, \vec{q})|^2 D_0^\mu(\vec{q}, i\omega_m), \quad (21)$$

where we introduce the bare fermion Green's function

$$G_0(\vec{k}, i\omega_n) = \frac{i\omega_n \tau_0 + \xi_{\vec{k}} \tau_3 + \Delta_{\vec{k}} \tau_1}{(i\omega_n)^2 - E_{\vec{k}}^2}, \quad (22)$$

with $E_{\vec{k}} = \sqrt{\xi_{\vec{k}}^2 + \Delta_{\vec{k}}^2}$ and the bare phonon Green's function

$$D_0^\mu(\vec{q}, i\omega_m) = \frac{1}{2} \left(\frac{1}{i\omega_m - \omega_q^\mu + i\eta} - \frac{1}{i\omega_m + \omega_q^\mu - i\eta} \right). \quad (23)$$

τ_l ($l = 1, 2, 3$) is the Pauli matrices, τ^0 is a unit matrix, and $\Delta_{\vec{k}} (= \Delta_0(\cos k_x - \cos k_y)/2)$ is the superconducting energy gap. The energy and momentum dependences of the occupied spectral density corresponding to the ARPES spectra are obtained by the (1,1)-component of the Green's function: $A(\vec{k}, \omega) = -\frac{1}{\pi} \text{Im}G_{11}(\vec{k}, i\omega_n \rightarrow \omega + i\delta)$. The calculated results are presented in Figs. 3 (a) and (b) for the off-diagonal coupling case, and in (c) and (d) for the diagonal case. The ARPES spectra show a kink structure below which both the spectral

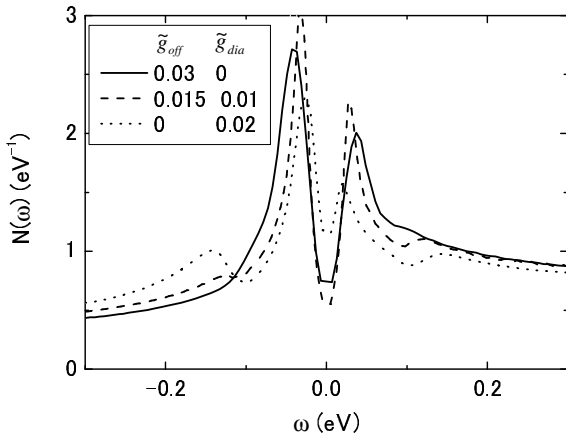


FIG. 4. Fermion density of states $N(\omega)$. The diagonal and off-diagonal coupling constants $(\tilde{g}_{off}, \tilde{g}_{dia})$ are chosen to be $(0.03\text{eV}, 0)$ for a solid line, $(0.015\text{eV}, 0.01\text{eV})$ for a broken line, and $(0, 0.02\text{eV})$ for a dotted line. Other parameters are $\omega_{ph} = 0.07\text{eV}$ and $\Delta_0 = 0.035\text{eV}$.

intensity and the quasi-particle lifetime remarkably increase. The kink energy in the superconducting state is less than $\Delta_0 + \omega_{ph}$ because of the d -wave gap. Although, at a glance, the kink effect in the spectra seems to be remarkable in the anti-nodal direction, this impression comes from the almost flat dispersion around $(\pi, 0)$ of the bare energy band. As shown later, the quasiparticle renormalization factor $Z(\vec{k}, \omega)$ dominating the velocity change at the kink energy is slightly weaker in the anti-nodal direction for the off-diagonal coupling case. This is consistent with the recent ARPES experiments where the quasiparticle velocity does not show a huge change at ω_{kink} around the anti-nodal direction, unlike the prediction in the magnetic mode calculations.^{20,29}

The tunneling density of states

$$N(\omega) = -\frac{1}{\pi N} \sum_{\vec{k}} \text{Tr} \text{Im}G(\vec{k}, i\omega_n \rightarrow \omega + i\delta), \quad (24)$$

are presented in Fig. 4. An asymmetrical shape of the spectra is attributed to the almost flat band around the $(\pi, 0)$ point below the fermi energy. Outside the superconducting gap, a dip and hump structure appears, being consistent with experiments.^{45,46} In the off-diagonal coupling case, the weak hump structure is located at $\pm(\Delta_0 + \omega_{ph})$. With increasing the diagonal-coupling parameter, this structure becomes pronounced, in particular, in the negative side, and the position of the structure shifts to the lower energy. It is seen simultaneously that for the strong diagonal coupling, the gap structure becomes shallow and is gradually collapsed.

The quasiparticle scattering rate deduced from the optical conductivity is calculated in the memory-function formalism. The optical conductivity is represented by utilizing the memory function $M_{\alpha\alpha}(\omega)$ which corresponds to the inverse of the energy-depend life-time $\tau(\omega)$ as

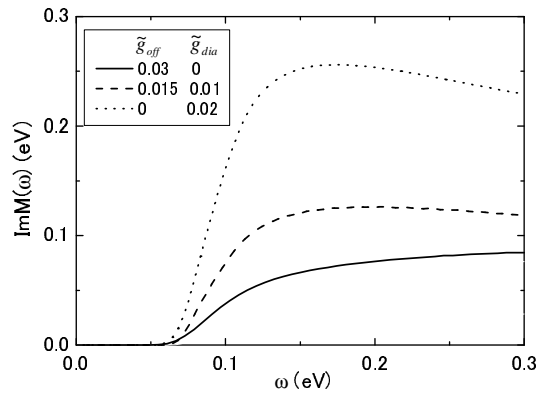


FIG. 5. Imaginary part of the memory function $\text{Im}M(\omega)$. The diagonal and off-diagonal coupling constants $(\tilde{g}_{off}, \tilde{g}_{dia})$ are chosen to be $(0.03\text{eV}, 0)$ for a solid line, $(0.015\text{eV}, 0.01\text{eV})$ for a broken line, and $(0, 0.02\text{eV})$ for a dotted line. Other parameters are $\omega_{ph} = 0.07\text{eV}$, $\Delta_0 = 0$ and $t = 0.3\text{eV}$. We use that $\chi_0 = 0.81ta^2$ calculated for the half-filled tight-binding model in the two-dimensional square lattice with NN electron hopping.

$$\sigma_{\alpha\alpha}(\omega) = \frac{i}{4\pi} \frac{\omega_P^2}{\omega + M_{\alpha\alpha}(\omega)}, \quad (25)$$

with the plasma frequency ω_P and the Cartesian coordinate α . The memory function $M_{\alpha\alpha}(\omega)$ is defined by⁴⁷

$$M_{\alpha\alpha}(\omega) = \frac{1}{\chi_0\omega} \{ \chi_{\alpha\alpha}(\omega) - \chi_{\alpha\alpha}(0) \}. \quad (26)$$

$\chi_{\alpha\alpha}(\omega)$ is the Fourier transform of the retarded Green's function of the operator \vec{A}_α defined by the equation of motion for the current operator j_α as $A_\alpha = [j_\alpha, H]$. Explicitly,

$$A_\alpha = -2ta \sum_{\vec{k}, \vec{q}, \sigma, \mu} \{ \sin a(k_\alpha + q_\alpha) - \sin ak_\alpha \} \times g^\mu(\vec{k}, \vec{q}) f_{\vec{k}+\vec{q}\sigma}^\dagger f_{\vec{k}\sigma} \left(b_{\vec{q}}^\mu + b_{-\vec{q}}^{\mu\dagger} \right), \quad (27)$$

where we consider the current between the NN sites. In the calculation of $M_{\alpha\alpha}(\omega)$, the correlation functions of fermion and phonon operators are evaluated for the non-interacting Hamiltonian. χ_0 in Eq. (26) is the static limit of the response function of j_α . The calculated $\text{Im}M(\omega)$ are shown in Fig. 5. $\text{Im}M(\omega) (\equiv \text{Im}M_{xx}(\omega) = \text{Im}M_{yy}(\omega))$ is rapidly depressed below ω_{ph} . Introducing the diagonal coupling, the scattering rate increases above the threshold energy and its reduction below the energy becomes steep. This large depression in the quasiparticle scattering rate deduced from the optical spectra is commonly observed in a variety of HTSC, e.g. LSCO, YBCO, Tl2201 and NCCO around $\omega = 400 \sim 800\text{cm}^{-1}$ (Ref. 27). This threshold energy is rather larger than the so-called pseudogap estimated in the inelastic neutron scattering, ARPES and tunneling spectra, and is close to the kink

energy related to ω_{ph} in the present scenario. Absolute values of the calculated $\text{Im}M(\omega)$ are compared with the experimental quasiparticle scattering rate. χ_0 is estimated in the two-dimensional tight-binding model with the NN electron hopping. Around the threshold energy, the experimental $\tau(\omega)^{-1}$ is about 2000cm^{-1} in underdoped Bi2212 and LSCO with $x = 0.14$, 1000cm^{-1} in NCCO, and 500cm^{-1} in overdoped Pb doped Bi2212.²⁷ These values are comparable to the present results of $\text{Im}M(\omega)$ in Fig. 5. That is, the electron-phonon interaction provides a large portion of the scattering rate in the optical region.

The memory function $\text{Im}M(\omega)$ at $\omega = 0$ corresponds to the scattering rate in the DC resistivity. The temperature dependence of $\text{Im}M(\omega = 0)$ is presented in Fig. 6. It is known that the scattering rate deduced from the experimental resistivity data is of the order of $2T$.⁴⁸ The calculated $\text{Im}M(0)$ gradually increases around $\omega_{ph}/5$ with increasing temperature, and its absolute value is rather smaller than $2T$. These results indicate that the phonon contribution is less dominant for $\tau(0)^{-1}$ in the resistivity, in contrast to the scattering rate in the optical region as mentioned above. It is noted that the superconducting gap Δ_0 is put to be zero in Figs. 5 and 6. When we introduce the finite Δ_0 to describe the pseudo-gap state, $\text{Im}M(0)$ will be further reduced due to the reduced final density of state.

The momentum dependences of the fermion renormalization factor $Z(\vec{k}, \omega) = (1 - \partial\Sigma(\vec{k}, \omega)/\partial\omega)^{-1}$ at $\omega = \Delta_0$ are presented in Figs. 7(a) and (b) for the off-diagonal and diagonal couplings, respectively. The broken lines indicate the fermi surface for $\xi_{\vec{k}}$. In the off-diagonal coupling case, $\text{Re}Z(\vec{k}, \omega = \Delta_0)$ is close to one around the $k_x + k_y = \pi$ line in the Brillouin zone, and is strongly reduced around $(0, 0)$ and (π, π) . In contrast, the momentum dependence is much weaker in the diagonal case, reflecting that the coupling constant $g_{dia}^{\mu}(\vec{k}, \vec{q})$ is independent of the electron-momentum \vec{k} as seen in Eq. (17). The calculated results for the off-diagonal coupling can explain the anisotropic quasiparticle scattering rate suggested in the recent ARPES experiments: Full width half maximum (FWHM) of the quasiparticle energy distribution curve is measured along the fermi surface in Pb-doped Bi2212 compound.⁴⁹ The reduction in FWHM on going away from the node is observed along both the bonding and antibonding quasi-particle bands. This experimental momentum dependence is consistent with the off-diagonal results shown in Fig. 7 (a), but is difficult to be explained by the magnetic excitation around $\vec{q} = (\pi, \pi)$ and the diagonal electron-phonon coupling.

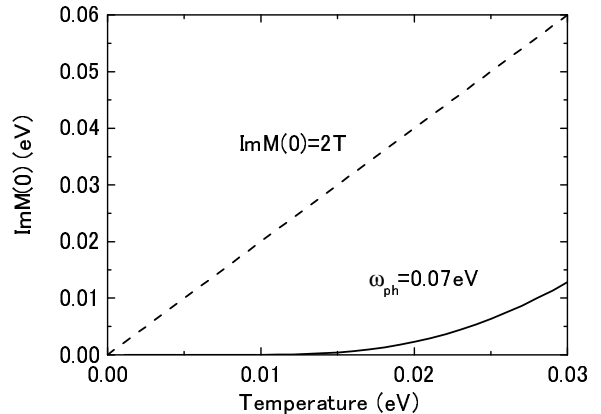


FIG. 6. Temperature dependence of the imaginary part of the memory function $\text{Im}M(\omega)$ at $\omega = 0$ (bold line). Broken line indicates a curve of $\text{Im}M(0) = 2T$. The diagonal and off-diagonal electron-phonon coupling constants, $(\tilde{g}_{off}, \tilde{g}_{dia})$, are chosen to be $(0.03\text{eV}, 0)$. Other parameters are $\omega_{ph} = 0.07\text{eV}$, $\Delta_0 = 0$ and $t = 0.3\text{eV}$. We use that $\chi_0 = 0.81ta^2$ calculated for the half-filled tight-binding model in the two-dimensional square lattice with NN electron hopping.

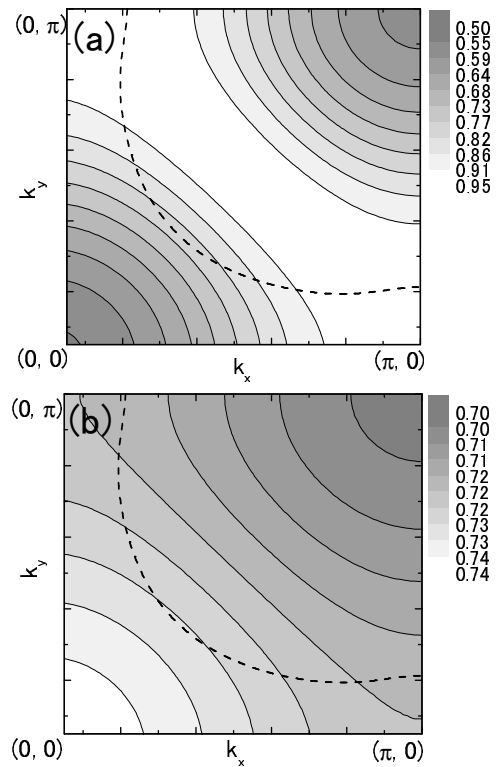


FIG. 7. Contour map of the real part of the fermion renormalization factor $\text{Re}Z(\vec{k}, \omega = \Delta_0)$ in the off-diagonal coupling case (a), and in the diagonal coupling case (b). Broken lines indicate the fermi surface in $\xi_{\vec{k}}$. The diagonal and off-diagonal electron-phonon coupling constants, $(\tilde{g}_{off}, \tilde{g}_{dia})$, are chosen to be $(0.03\text{eV}, 0)$ in (a), and $(0, 0.02\text{eV})$ in (b). Other parameters are $\omega_{ph} = 0.07\text{eV}$ and $\Delta_0 = 0.035\text{eV}$.

III. VERTEX CORRECTION

A. Formulation of the Vertex Correction

We now go beyond the slave-boson mean field treatment in the electron-phonon interaction in $t - J$ model. This is carried out by taking into account the fluctuations around the mean fields, leading to the vertex correction in the fermion-phonon interaction. We formulate this effective electron-phonon coupling in the SU(2) slave boson theory^{35–37} which imposes that the fermion operators

$$\Psi_{i\uparrow} = \begin{pmatrix} f_{i\uparrow} \\ f_{i\downarrow}^\dagger \end{pmatrix}, \quad \Psi_{i\downarrow} = \begin{pmatrix} f_{i\downarrow} \\ -f_{i\uparrow}^\dagger \end{pmatrix}, \quad (28)$$

are taken to be the local SU(2) doublet. This is an exact symmetry in the $t - J$ model at half filling³⁵ where the two order parameters, i.e., the fermion hopping χ_{ij} ($= \sum_\sigma f_{i\sigma}^\dagger f_{j\sigma}$) and the fermion paring Δ_{ij} ($= f_{i\uparrow} f_{j\downarrow} - f_{i\downarrow} f_{j\uparrow}$), become equivalent. Even at the finite but small doping, it is expected that the low energy physics is captured by this picture. The generalized SU(2) theory away from the half filling is provided by introducing the SU(2) doublet for bosons $\hat{h}_i = (h_{1i}, h_{2i})^t$.³⁶ Then, the physical electron operator is $c_{i\sigma} = \hat{h}_i^\dagger \Psi_{i\sigma}$ with constraints $\frac{1}{2} \sum_\sigma \Psi_{i\sigma}^\dagger \vec{\tau} \Psi_{i\sigma} + \hat{h}_i^\dagger \vec{\tau} \hat{h}_i = 0$. Three bosonic fields a_i^l ($l = 1 \sim 3$) are required as Lagrange multipliers to keep these constraints. It is known that the Lagrangian in the SU(2) theory is rewritten as being similar to that in the U(1) theory. This is carried out by representing the two-component bosons as a SU(2) rotation, denoted by the rotation matrix g_i , of the standard slave-boson h_i .³⁸ By integrating out the variable g_i , the Lagrangian for the $t - J$ model in the SU(2) theory associated with the electron-phonon interaction is obtained as

$$L = L_{tJ} + L_{el-ph}, \quad (29)$$

where L_{tJ} is the electronic part:

$$\begin{aligned} L_{tJ} = & \frac{J}{2} \sum_{\langle ij \rangle} \text{Tr}[U_{ij}^* U_{ij}] + \frac{J}{2} \sum_{\langle ij \rangle, \sigma} (\Psi_{i\sigma}^\dagger U_{ij} \Psi_{j\sigma} + H.c.) \\ & + \frac{1}{2} \sum_{i, \sigma} \Psi_{i\sigma}^\dagger (\partial_\tau \tau_0 - i a_i^l \tau_l) \Psi_{i\sigma} \\ & + \sum_i h_i^\dagger (\partial_\tau - i a_i^3 + \mu) h_i \\ & - t \sum_{\langle ij \rangle, \sigma} (f_{i\sigma}^\dagger f_{j\sigma} h_i h_j^\dagger + H.c.), \end{aligned} \quad (30)$$

with a 2×2 matrix

$$U_{ij} = \begin{pmatrix} -\chi_{ij}^*, & \Delta_{ij} \\ \Delta_{ij}^*, & \chi_{ij} \end{pmatrix}. \quad (31)$$

The second term in Eq. (29) is the the fermion-phonon interaction:

$$\begin{aligned} L_{el-ph} = & \frac{1}{\sqrt{N}} \sum_{\vec{k}, \vec{q}, \mu, \sigma} g^\mu(\vec{k}, \vec{q}) \Psi_{\vec{k}+\vec{q}\sigma}^\dagger \tau_3 \Psi_{\vec{k}\sigma} \\ & \times \frac{1}{2} (b_{-\vec{q}}^{\mu\dagger} + b_{\vec{q}}^\mu), \end{aligned} \quad (32)$$

which is nothing but the Hamiltonian Eq. (15). From now on, we focus on the off-diagonal electron-phonon coupling in $g^\mu(\vec{k}, \vec{q})$ of the present interest.

The fluctuations around the mean-field saddle-points in the SU(2) theory are examined, in detail in Ref. 37, as the low-lying collective modes in the superconducting ground state. For the fermion hopping and the fermion paring, as well as the slave boson and the Lagrange multipliers, we introduce small deviations from the saddle-points;

$$\begin{aligned} \chi_{ij} &= \chi_0 + \delta \chi_{ij}, \\ \Delta_{ij} &= \Delta_0 (-1) \eta_l + \delta \Delta_{ij}, \\ h_i &= r_0 (1 + \delta r_i), \\ ia_i^l &= \delta_{l3} \lambda_0 + i \delta a_i^l. \end{aligned} \quad (33)$$

$\eta_l = (1, -1)$ for a direction of the bond $l = (x, y)$. We adopt the radial gauge where h_i is chosen to be real and its phase degree of freedom is absorbed in the Lagrange multipliers. Up to the quadratic fluctuations, we have a fermionic part of the Lagrangian as

$$L_{tJ} = L_{MF} + L_1 + L_2 + L_0, \quad (34)$$

with the constant term L_0 . L_{MF} is the mean-field part

$$L_{MF} = -\frac{1}{2N} \sum_{\vec{k}, \sigma} \Psi_{\vec{k}\sigma}^\dagger (\partial_\tau \tau_0 - \xi_{\vec{k}} \tau_3 - \Delta_{\vec{k}} \tau_1) \Psi_{\vec{k}\sigma}, \quad (35)$$

where we define the mean-field quasiparticle energy

$$\xi_{\vec{k}} = - (t_{\vec{k}} + J \chi_{\vec{k}} + \lambda_0), \quad (36)$$

with $\chi_{\vec{k}} = 2J\chi_0(\cos k_x + \cos k_y)$ and $\Delta_{\vec{k}} = 2J\Delta_0(\cos k_x - \cos k_y)$. The conventional definition of the superconducting gap Δ corresponds to $2J\Delta_0$. The bare fermion energy is considered up to the next NN hopping as $t_{\vec{k}} = 2r_0^2 \{t(\cos ak_x + \cos ak_y) + t_1 \cos ak_x \cos ak_y\}$. The mean-field solutions, χ_0 , Δ_0 and λ_0 , are determined by the saddle-point equations:

$$\chi_0 = -\frac{1}{2N} \sum_{\vec{k}} \frac{\xi_{\vec{k}}}{E_{\vec{k}}} \gamma_{\vec{k}}, \quad (37)$$

$$\Delta_0 = \frac{1}{N} \sum_{\vec{k}} \frac{\Delta_0}{E_{\vec{k}}} J \beta_{\vec{k}}^2, \quad (38)$$

$$\lambda_0 = \frac{1}{N} \sum_{\vec{k}} \frac{2t\xi_{\vec{k}}}{E_{\vec{k}}} \gamma_{\vec{k}}, \quad (39)$$

with $E_{\vec{k}} = \sqrt{\xi_{\vec{k}}^2 + \Delta_{\vec{k}}^2}$, $\beta_{\vec{k}} = \cos k_x - \cos k_y$ and $\gamma_{\vec{k}} = \cos k_x + \cos k_y$. The calculations in Sec. III are based

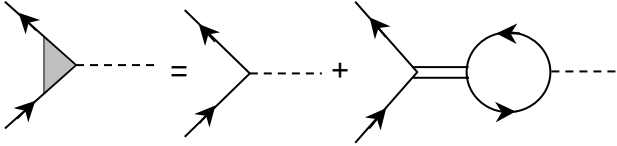


FIG. 8. Feynman diagram for the effective electron-phonon interaction vertex. Bold lines, double lines and broken lines indicate the fermion propagators $G_0(\vec{k}, i\omega_n)$, the bare collective-mode propagators $G_{J0}(\vec{q}) = M_J(\vec{q})^{-1}$, and the phonon propagators $D(\vec{q}, i\omega_m)$, respectively.

on $L_{MF} + L_{el-ph}$ where $\xi_{\vec{k}}$ is obtained by the tight-bind fitting in spite of Eq. (36). The linear coupling of the fluctuation with the fermionic degree of freedom is described by the second term in Eq. (34):

$$L_1 = \frac{1}{\sqrt{2N}} \sum_{\vec{k}, \vec{q}, \sigma} \Psi_{\vec{k}+\vec{q}\sigma}^\dagger \left(\vec{x}_{\vec{q}} \cdot \vec{f}_{\vec{k}, \vec{k}+\vec{q}} \right) \Psi_{\vec{k}\sigma}. \quad (40)$$

$(\vec{x}_{\vec{q}})_\nu$ and $(\vec{f}_{\vec{k}, \vec{k}+\vec{q}})_\nu$ ($\nu = 1 \sim 12$) are the fluctuations with 12 components and their structure factors, respectively, defined as

$$\vec{x}_{\vec{q}} = \left(\delta\chi''_{\vec{q}x}, \delta\chi''_{\vec{q}y}, \delta\Delta''_{\vec{q}x}, \delta\Delta''_{\vec{q}y}, \delta\Delta'_{\vec{q}x}, \delta\Delta'_{\vec{q}y}, \delta\chi'_{\vec{q}x}, \delta\chi'_{\vec{q}y}, \delta a_{\vec{q}}^1, \delta a_{\vec{q}}^2, \delta a_{\vec{q}}^3, \delta r_{\vec{q}} \right), \quad (41)$$

and

$$\vec{f}_{\vec{k}, \vec{k}+\vec{q}} = \left(-2JS_x\tau_0, -2JS_y\tau_0, 2JC_x\tau_1, 2JC_y\tau_1, -2JC_x\tau_2, -2JC_y\tau_2, -2JC_x\tau_3, -2JC_y\tau_3, -i\tau_1, -i\tau_2, -i\tau_3, -(\vec{t}_{\vec{k}} + \vec{t}_{\vec{k}+\vec{q}})\tau_3 \right), \quad (42)$$

with abbreviations $S_l = \sin(k_l + q_l/2)$ and $C_l = \cos(k_l + q_l/2)$ for $l = (x, y)$. $\delta\chi_{\vec{q}l} (= \delta\chi'_{\vec{q}l} + i\delta\chi''_{\vec{q}l})$ and $\delta\Delta_{\vec{q}l} (= \delta\Delta'_{\vec{q}l} + i\delta\Delta''_{\vec{q}l})$ are the Fourier transforms of $\delta\chi_{ij}$ and $\delta\Delta_{ij}$, respectively, where l indicates a direction of the bond connecting site i and site j . The third term L_2 in Eq. (34) is the quadratic term of the fluctuations. Explicitly,

$$L_2 = -2ir_0^2 \sum_{\vec{k}} \delta a_{\vec{k}}^3 \delta r_{-\vec{k}} - r_0^2 \sum_{\vec{k}} (t\beta_{\vec{k}}\lambda_1 + t_1 \cos ak_x \cos ak_y \lambda_2 - \lambda_0) |\delta r_{\vec{k}}|^2 + J \sum_{\vec{k}, l=(x,y)} (|\delta\chi_{\vec{k}l}|^2 + |\delta\Delta_{\vec{k}l}|^2), \quad (43)$$

with $\lambda_1 = -\sum_{\vec{k}} \frac{\xi_{\vec{k}} \gamma_{\vec{k}}}{E_{\vec{k}}}$ and $\lambda_2 = -2 \sum_{\vec{k}} \frac{\xi_{\vec{k}} \cos ak_x \cos ak_y}{E_{\vec{k}}}$.

The effective fermion-phonon coupling is obtained in this scheme. The dynamics of the fluctuations $\vec{x}_{\vec{q}}$ is governed through the interaction between the fluctuations and fermion. By integrating out the fermionic degree of freedom in the action, we obtain the RPA-type summation of the bare Green's function for the fluctuations

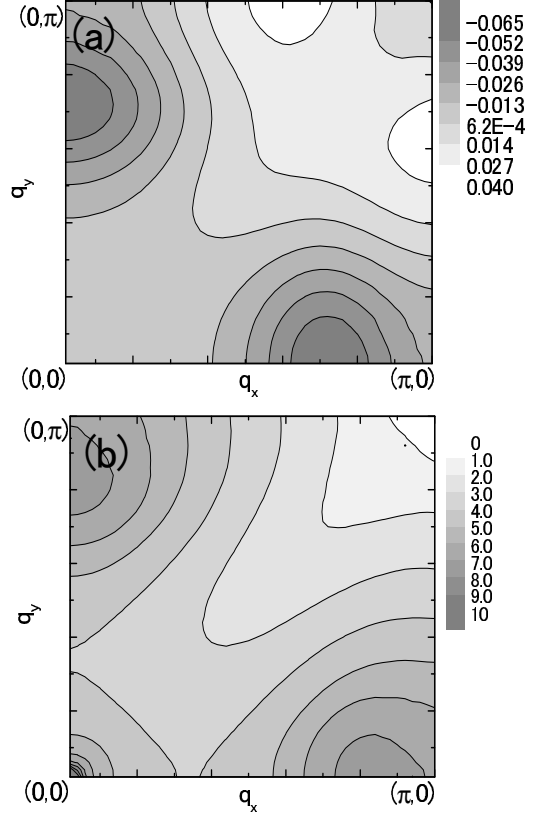


FIG. 9. Contour map of (a) the effective paring interaction $F(\vec{q})$ in the off-diagonal coupling case with the vertex correction, and (b) the vertex function $\Gamma(\vec{q}, 0)$. Parameters are chosen to be $t/J = 3$, $t_1/J = -1.5$, $\tilde{g}_{off}/J = 0.1$, $\omega_{ph}/J = 0.5$ and $x = 0.1$. Numerical data are plotted in a unit of J .

$G_{J0}(\vec{q}) = F.T. \langle \vec{x}_{\vec{q}}(\tau) \vec{x}_{-\vec{q}}^\dagger(0) \rangle_0$, where $\langle \dots \rangle_0$ indicates an expectation in L_2 , and the fermion polarization function $M_F(\vec{q}, i\omega_n)$ defined by

$$M_F(\vec{q}, i\omega_n) = \sum_{\vec{k}, \omega_m} \vec{f}_{\vec{k}+\vec{q}, \vec{k}} G_0(\vec{k}, i\omega_m) \times G_0(\vec{k} + \vec{q}, i\omega_m + i\omega_n) \vec{f}_{\vec{k}+\vec{q}, \vec{k}}. \quad (44)$$

$G_0(\vec{k}, i\omega_m)$ is the bare fermion Green's function calculated by L_{MF} (Eq. (35)). The effective fermion-phonon vertex is now given by the bare interaction plus the correction due to the collective modes of the fluctuations (Fig. 8). Explicitly, the coupling constant is

$$\vec{\eta}_{\vec{q}}^\mu(\vec{k}, \vec{q}; i\omega_n) = \vec{\eta}_{\vec{q}}^\mu \cdot \Lambda(\vec{q}, i\omega_n) \cdot \vec{f}_{\vec{k}, \vec{k}+\vec{q}}. \quad (45)$$

$\vec{\eta}_{\vec{q}}^\mu$ is a vector with 12 components defined as

$$\left(\vec{\eta}_{\vec{q}}^\mu \right)_\nu = 4ig_{off} J^{-1} \frac{1}{\sqrt{2N} M \omega_{\vec{q}}^\mu} \sin\left(\frac{q_\mu}{2}\right) \times \left\{ \delta_{\nu 7} \cos\left(\frac{q_x}{2}\right) + \delta_{\nu 8} \cos\left(\frac{q_y}{2}\right) \right\}. \quad (46)$$

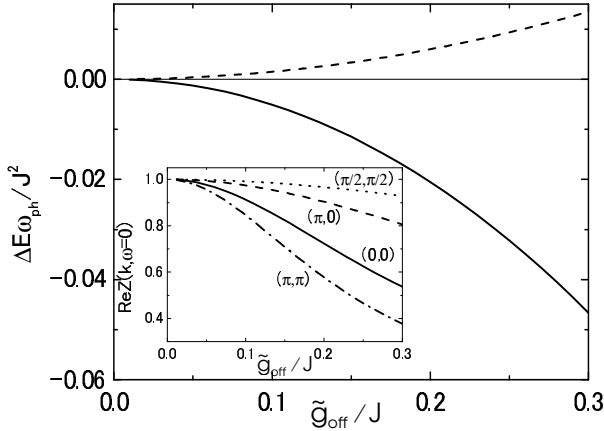


FIG. 10. Superconducting condensation energy ΔE . Solid and broken lines indicate $\Delta E\omega_{ph}/J^2$ with and without the vertex correction, respectively. The inset shows the real part of the fermion renormalization factor $\text{Re}Z(\vec{k}, 0)$. Parameters are chosen to be $t/J = 3$, $t_1/J = -1.5$, $\omega_{ph}/J = 0.5$ and $x = 0.1$.

The finite components at $l = 7$ and 8 in $\eta_{\vec{q}}^{\mu}$ are attributed to the fact that the fermion-phonon vertex is proportional to τ_3 . $\Lambda(\vec{q}, i\omega_n)$ is the energy-dependent vertex function of a 12×12 matrix

$$\Lambda(\vec{q}, i\omega_n) = \frac{M_J(\vec{q})}{M_J(\vec{q}) + M_F(\vec{q}, i\omega_n)}, \quad (47)$$

represented by the inverse of the bare fluctuation Green's function $M_J(\vec{q}) = G_{J0}(\vec{q})^{-1}$ and the renormalized fluctuation Green's function

$$G_J(\vec{q}, i\omega_n) = \frac{1}{M_J(\vec{q}) + M_F(\vec{q}, i\omega_n)}, \quad (48)$$

which describes dynamics of the collective modes in the superconducting ground state.

B. numerical results with vertex correction

We show, in this section, the numerical results obtained by taking into account the vertex correction for the electron-phonon interaction in Eq. (45). As shown below, the effects of the vertex correction depends strongly on the physical quantities. Some of them are seriously modified, while others are insensitive to the vertex correction. The parameter values are given in a unit of J , and we use $t/J = 3$, $t_1/J = -1.5$, $\tilde{g}_{off}/J = 0.1$, $x = 0.1$ and $\omega_{ph}/J = 0.5$. The holon is assumed to be condensed and its amplitude r_0 is taken to be \sqrt{x} . The obtained mean-filed solutions are $\Delta_0 = 0.278$ and $\chi = 0.370$.

The vertex correction is a crucial for the calculation of the paring function and the condensation energy. The momentum dependence of the effective paring interaction $F(\vec{q})$ is obtained by Eq. (20) where $g^{\mu}(\vec{k}, \vec{q})$ is replaced

by the effective coupling constant $\hat{g}^{\mu}(\vec{k}, \vec{q}; i\omega_n = 0)$ defined in Eq. (45). The numerical results are presented in Fig. 9 (a). The vertex correction does not only enhance magnitude of the attractive interaction, as will be discussed in more detail below, but also shifts the minimum region from $(\pi, 0)$ to $(\pi(1 - \delta), 0)$ with $\delta \cong 0.3$. This is exactly the momentum region where the minimum of the anomalous dispersion is observed in the inelastic neutron scattering.^{14,15} We plot, in Fig. 9 (b) the contour map of the absolute value of the vertex function $\Gamma(\vec{q}, \omega = 0)$ defined by

$$\Gamma(\vec{q}, i\omega_n) = \sum_{\nu} \left\{ \Lambda(\vec{q}, i\omega_n)_{7\nu} \cos\left(\frac{q_x}{2}\right) + \Lambda(\vec{q}, i\omega_n)_{8\nu} \cos\left(\frac{q_y}{2}\right) \right\}. \quad (49)$$

We resolve this vertex function into the contribution from the collective modes by following the classification in Ref. 39. The strong intensity around $\vec{q} = (0, 0)$ in $\Gamma(\vec{q}, 0)$ is attributed to the Goldstone mode, i.e. the uniform collective phase mode of the superconducting order parameter. This eigen vector is denoted as

$$\delta\alpha_{U\vec{q}} = \delta\Delta''_{\vec{q}x} - \delta\Delta''_{\vec{q}y}, \quad (50)$$

where α indicates the overall phase of χ_{ij} and Δ_{ij} around the staggered-flux order parameters. This contribution in the effective fermion-phonon interaction is, however, irrelevant, because of the factor $\sin(q_{\mu}/2)$ in Eq. (46) and also because the long range Coulomb interaction lifts up the frequency to plasma energy in real system. A large contribution around $(\pi, 0)$ is mainly attributed to the two collective modes, i.e. the amplitude mode

$$\delta A_{\vec{q}l} = \Delta_0 \delta\Delta'_{\vec{q}l} + \chi_0 \delta\chi'_{\vec{q}l}, \quad (51)$$

for $l = (x, y)$ representing the amplitude fluctuation for the order parameter $|\chi_{\vec{q}l}|^2 + |\Delta_{\vec{q}l}|^2$, and the transverse and longitudinal ϕ gauge modes

$$\phi_{T\vec{q}} = \chi_0 \delta\Delta'_{\vec{q}y} - \Delta_0 \delta\chi'_{\vec{q}y}, \quad (52)$$

$$\phi_{L\vec{q}} = \chi_0 \delta\Delta'_{\vec{q}x} + \Delta_0 \delta\chi'_{\vec{q}x}. \quad (53)$$

The amplitude fluctuation $\delta A_{\vec{q}l}$ has a large intensity around $(\pi, 0)$ and $(0, \pi)$, and increases the effective paring interaction $F(\vec{q})$ around these momenta. This may be a remnant of the instability toward the columnar-dimer state which is well known in the insulating case.^{50,51} The ϕ modes are the amplitude modes with the out-of-phase fluctuation for the fermion hopping χ_{ij} and paring Δ_{ij} . The longitudinal ϕ gauge mode $\phi_{L\vec{q}}$ shows a large intensity in the low energy region around $\vec{q} = (\pi/2, \pi)$, in addition to the peak structure around $\vec{q} = (\pi/2, \pi)$ suggested in Ref. 39. This mode shifts the minimum point of $F(\vec{q})$ from $(\pi, 0)$ without vertex correction to $(\pi(1 - \delta), 0)$ with $\delta \cong 0.3$ in the low energy region.

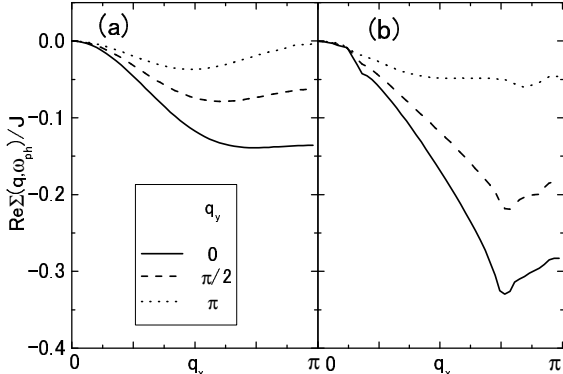


FIG. 11. Real part of the phonon self-energy without the vertex correction (a), and with the vertex correction (b). Parameters are chosen to be $t/J = 3$, $t_1/J = -1.5$, $\tilde{g}_{off}/J = 0.1$, $\omega_{ph}/J = 0.5$ and $x = 0.1$.

The superconducting condensation energy ΔE is given by the expectation value of the effective BCS Hamiltonian, i.e. Eq. (20) where the vertex correction is included in the coupling constant. The numerical results of ΔE as function of the bare off-diagonal coupling constant g_{off} is presented in Fig. 10 associated with the renormalization factor $\text{Re}Z(\vec{k}, \omega = 0)$. As shown in the broken line in Fig. 10, the condensation energy is positive in the case without vertex correction. Thus, the d -wave superconductivity due to the present LO phonon is stabilized by introducing the vertex correction. By considering the velocity ratio R_v across the kink energy, a value of \tilde{g}_{off}/J is expected to be 0.2 where $\text{Re}Z(\vec{q}, 0)$ is about 0.6 \sim 0.8 at $\vec{q} = (0, 0)$ and (π, π) , and $\Delta E \omega_{ph}/J^2 = -0.02$ is converted into about 40K, taking $J = 100\text{meV}$. The actual condensation energy is of the order of 7K for optimally doped YBCO⁵², which is smaller than this value. One can consider various reasons for this discrepancy. (i) the estimation of the condensation energy has an uncertainty due to the subtle subtraction of the phonon contribution, (ii) there are other mechanisms to reduce the pairing and hence the condensation energy which are not considered here, and (iii) the determination of $\text{Re}Z(\vec{k}, 0)$, i.e. the electron-phonon coupling constant λ from the experimental velocity ratio may be overestimated.

The momentum dependence of the phonon self-energy is presented in Fig. 11. The phonon self-energy $\Sigma_{ph}(\vec{q}, \omega = \omega_{ph})$ is calculated from the fermion bubble of the bare fermion Green's function $G_0(\vec{k}, \omega)$ associated with the vertex correction. We consider the phonon mode where the oxygen ions vibrate along the x direction. As shown in the Fig. 11(a), the softening of the phonon dispersion is remarkably seen along the $(q_x, 0)$ direction with $q_y \lesssim \pi/2$. This is the region where the softening of the oxygen vibrational LO phonon mode is reported in the inelastic neutron scattering experiments. The phonon softening is gradually reduced with increasing q_y , and along the (q_x, π) direction, the phonon frequency is al-

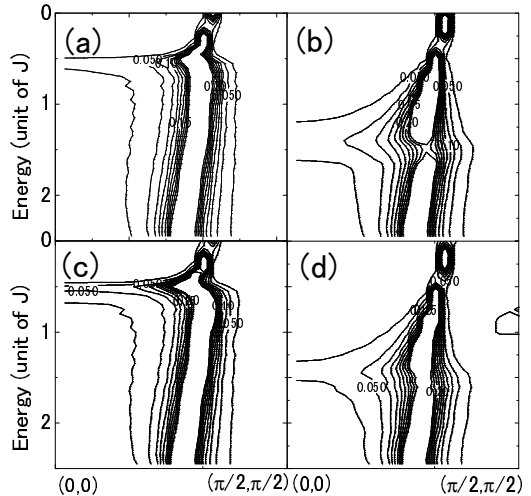


FIG. 12. Contour map of the fermion spectral density $A(\vec{k}, \omega)$ along the nodal direction without the vertex correction (a) and (b), and with the correction (c) and (d). (a) and (c) are for the spectra with $\Delta_0 = 0$, and (b) and (d) are for the spectra with $\Delta/J = 2\Delta_0/J = 0.57$. Parameters are chosen to be $t/J = 3$, $t_1/J = -1.5$, $\tilde{g}_{off}/J = 0.1$, $\omega_{ph}/J = 0.5$ and $x = 0.1$. The dispersion relation of the quasi-particle energy $\xi_{\vec{k}}$ is chosen to be the same form with that in Fig. 3. Numerical data are plotted in a unit of J^{-1} .

most unrenormalized. By introducing the vertex correction (Fig. 11(b)), these tendency become significant. Although the qualitative feature of the calculated phonon softening is consistent with the experiments, absolute value of the frequency shift is much larger than the observation, in particular with the vertex correction. This may indicate that the adopted electron-phonon coupling constant is overestimated, as mentioned previously, and a further refinement for the vertex correction is required for more quantitative discussion.

On the other hand, the electronic spectra are not sensitive to the vertex correction as shown below. Figures 12 show the ARPES spectra along the nodal direction with and without the vertex correction. The energy dependence of the vertex function is taken into account in the calculation of the spectra. Comparing Figs. 12 (a), (b) and (c), (d), it is concluded that the vertex correction does not play significant roles in the ARPES spectra. This is because the electronic self-energy is given by the contributions from the wide range of the phonon momentum \vec{q} , and the vertex correction is large only in a rather limited \vec{q} region as shown in Fig. 9(b). This fact is also consistent with the shift of the kink position in the superconducting state; the kink energy shifts from ω_{ph} to $\omega_{ph} + 2\alpha\Delta$ with $\alpha \cong 0.7$. However, this does not reproduce the experimental observation that the kink position does not change across the superconducting transition.

We present, in Fig. 13, a contour map for the renormalization factor for fermion $\text{Re}Z(\vec{k}, \omega = 0)$ with the vertex correction. In the case where the vertex correction is

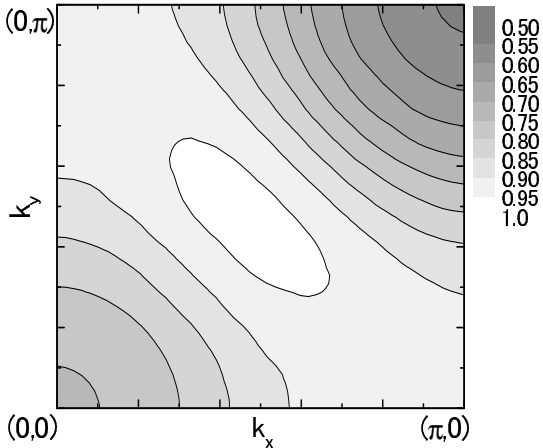


FIG. 13. Contour map of the real part of the fermion renormalization factor $\text{Re}Z(\vec{k}, 0)$ in the off-diagonal coupling with the vertex correction. Parameters are chosen to be $t/J = 3$, $t_1/J = -1.5$, $\tilde{g}_{off}/J = 0.1$, $\omega_{ph}/J = 0.5$ and $x = 0.1$.

included, the essence of the momentum dependence of $\text{Re}Z(\vec{k}, 0)$ pointed out in the previous section, i.e. the large renormalization around $\vec{k} = (0, 0)$ and (π, π) , remains, although $\text{Re}Z(\vec{k}, 0)$ around $\vec{k} = (\pi, \pi)$ is slightly reduced.

IV. DISCUSSION AND CONCLUSIONS

The interplay between the electron-phonon interaction and strong electronic correlation is one of the most important issues in many systems such as cuprates, manganites, and C_{60} . Especially in cuprates, it has been often claimed that the strong correlation dominates to hide or reduce the electron-phonon interaction. This seems to be true for the diagonal coupling of phonon because the charge density fluctuation is suppressed by the Mott physics. This is assumed also in the present paper neglecting the diagonal electron-phonon coupling. However it also plays an important role in the dynamics of the hole observed in the ARPES of the undoped cuprates⁵³ because the photo-doped hole is subject to the rather strong coupling to the breathing phonon mode. We believe that this electron-phonon interaction is the origin of the anomalously large width of the ARPES spectra.⁵⁴

Now some remarks are in order on other works on the electron-phonon interaction in cuprates. Rösch and Gunnarsson²⁵ studied the electron-phonon interaction in the $t - J$ model in a similar way estimating the value of the coupling constants from the r -dependence of the transfer integral and the inter-site Coulomb interaction between the O and Cu ions (r is the distance between these two ions). The off-diagonal coupling constant is an order of magnitude smaller than what we estimated, while the diagonal-coupling constant is huge of the order of 0.25eV. Therefore they concluded the diagonal

coupling is the dominant mechanism of electron-phonon interaction in cuprates, even though it is reduced considerably by the same mechanism we discussed in this paper. However the small value of off-diagonal coupling constant is due to the rather subtle cancellation between two terms, and might change in a more realistic calculation. Also the vertex correction strongly enhances the off-diagonal coupling.

Huang *et al.*²³ recently studied the electron-phonon vertex correction for the diagonal coupling due to the Coulomb correlation, and found that the large momentum transfer scattering is reduced considerably while that of small momentum transfer is enhanced. This feature is consistent with the earlier analytic studies on the vertex correction.⁴⁰ The important point made in that paper²³ is that the interaction between the quasi-particle and phonon is *enhanced* by the electron correlation because of the enhanced density of states. This might have an important implication for the kink structure observed in the $(\pi, 0)$ momentum region.³⁴

In summary, we have studied the electron-phonon interaction in HTSC cuprates motivated by the recent ARPES experiments. The off-diagonal electron-phonon coupling, which modulates the hopping integral of the Zhang-Rice singlet and the superexchange interaction, is relevant in the small doping region. We formulate the vertex correction beyond the mean-filed slave boson theory. As well as the slave boson and the Langrange multiplier, the fluctuations for the fermion hopping and paring lead to the collective modes in the superconducting state.³⁹ Thus, the dynamics of the collective modes dominates the vertex function for the electron-phonon interaction. A characteristics in the off-diagonal coupling constant $g_{off}^\mu(\vec{k}, \vec{q})$ are consistent with several \vec{k} (electron momentum) and \vec{q} (phonon momentum) dependent experiments; the anisotropy in the quasiparticle renormalization reflecting the momentum-dependent velocity ratio across the kink and its peak-width, and the phonon momentum dominating the strong electron-phonon coupling. With the vertex correction, the attractive interaction increases and the phonon momentum induces the interaction shifts to $(\pi(1 - \delta), 0)$ with $\delta \cong 0.3$. These changes are caused by the amplitude fluctuation mode and the ϕ gauge mode, that is, the collective fluctuations of the order parameter amplitude $|\chi_{ij}|^2 + |\Delta_{ij}|^2$, and its out-of-phase fluctuation mode, respectively. However, the kink position in the ARPES spectra shifts from ω_{ph} to $\omega_{ph} + 2\alpha\Delta$ across T_c in our calculation, while it does not in the experiments. The resolution of this discrepancy is left for future studies.

It is evident that the strong electron correlation plays the major role in the physics of HTSC cuprates, and the role of the phonon is also modified by it. Some specific channel of the electron-phonon interaction is selected to be enhanced by the strong correlation, and this will avoid the competition with the magnetic mechanism working in the different momentum regions. Therefore it seems that

the electron correlation and the electron-phonon interaction seems to collaborate to enhance the *d*-wave pairing. The role of the other phonons besides the half-breathing mode studied here, is left for future investigations.

ACKNOWLEDGMENTS

We would like to acknowledge Z. -X. Shen, A. Lanzara, T. Cuk, A. Fujimori, T. Egami, M. Tachiki, W. Hanke, S. Sugai, and O. Gunnarsson for their stimulus discussions. This work is supported by KAKENHI from MEXT. Part of the numerical calculation has been performed by the supercomputing facilities in IMR, Tohoku University.

¹ G. Baskaran, Z. Zou, and P. W. Anderson, *Sol. Stat. Comm.* **63**, 973 (1987).

² G. Kotliar, and J. Liu, *Phys. Rev. Lett.* **61**, 1784 (1988).

³ Y. Suzumura, Y. Hasegawa, and H. Fukuyama, *Jour. Phys. Soc. Jpn.* **57**, 2768 (1988).

⁴ N. Nagaosa, and P. A. Lee, *Phys. Rev. Lett.* **64**, 2450 (1990), and P. A. Lee, and N. Nagaosa, *Phys. Rev. B* **46**, 5621 (1992).

⁵ L. B. Ioffe, and A. I. Larkin, *Phys. Rev. B* **39**, 8988 (1989).

⁶ K. Yonemitsu, A. R. Bishop, and J. Lorenzana, *Phys. Rev. Lett.* **69**, 965 (1992).

⁷ S. Ishihara, T. Egami, and M. Tachiki, *Phys. Rev. B* **53**, 3163 (1997).

⁸ G. Khaliullin, and P. Horsch, *Phys. Rev. B* **54**, R9600 (1996).

⁹ A. Nazarenko, and E. Dagotto, *Phys. Rev. B* **53**, R2987 (1996).

¹⁰ B. Normand, H. Kohno, and H. Fukuyama, *Phys. Rev. B* **53**, 856 (1996).

¹¹ L. Boeri, E. Cappelluti, C. Grimaldi, and L. Pietroneto, *Inter. Jour. Mod. Phys. B* **14**, 2970 (2000).

¹² M. K. Crawford, M. N. Kunchur, W. E. Farneth, E. M. McCarron III, and S. J. Poon, *Phys. Rev. B* **41**, 282 (1990).

¹³ G. -M. Zhao, M. B. Hunt, H. Keller, and K. A. Müller, *Nature* **385**, 236 (1997), and G.-M. Zhao, H. Keller, and K. Conder, *cond-mat/0204447*.

¹⁴ R. J. McQueeney, Y. Petrov, T. Egami, M. Yethiraj, G. Shirane, and Y. Endoh, *Phys. Rev. Lett.* **82**, 628 (1999).

¹⁵ L. Pintschovius, and M. Braden, *Phys. Rev. B* **60**, R15 039 (1999), and M. Braden, W. Reichardt, S. Shiryaev, and S. N. Barilo, *Physica C* **378-381**, 89 (2002).

¹⁶ T. Fukuda, J. Mizuki, K. Ikeuchi, K. Yamada, M. Fujita, Y. Endoh, A. Q. R. Baron, T. Tsutsui, and Y. Tanaka, (unpublished).

¹⁷ P. V. Bogdanov, A. Lanzara, S. A. Keller, X. J. Zhou, E. D. Liu, W. J. Zheng, G. Gu, J. -I. Shimoyama, K. Kishio, H. Ikeda, R. Yoshizaki, Z. Hussain, and Z. -X. Shen, *Phys. Rev. Lett.* **85**, 2581 (2000).

¹⁸ A. Kaminski, M. Randeria, J. C. Campuzano, M. R. Norman, H. Fretwell, J. Mesot, T. Sato, T. Takahashi, and K. Kadowaki, *Phys. Rev. Lett.* **86**, 1070 (2001).

¹⁹ P. D. Johnson, T. Valla, A. V. Fedorov, Z. Yusof, B. O. Wells, Q. Li, A. R. Moodenbaugh, G. D. Gu, N. Koshizuka, C. kendziora, Sha Jian, and D. G. Hink, *Phys. Rev. Lett.* **87**, 177077 (2001).

²⁰ A. Lanzara, P. V. Bogdanov, X. J. Zhou, S. A. Keller, D. L. Feng, E. D. Lu, T. Yoshida, H. Eisaki, A. Fujimori, K. Kishio, J. -I. Shimoyama, T. Noda, S. Uchida, Z. Hussain, and Z. -X. Shen, *Nature* **412**, 510 (2001).

²¹ Z. -X. Shen, A. Lanzara, S. Ishihara, and N. Nagaosa, *Phil. Mag.* **82**, 1349 (2002).

²² M. Tachiki, M. Machida, and T. Egami, *Phys. Rev. B* **67**, 174506 (2003).

²³ Z. B. Huang, W. Hanke, E. Arigoni, and D. J. Scalapino, *cond-mat/03006131*.

²⁴ E. Schachinger, J. J. Tu, and J. P. Carbotte, *Phys. Rev. B* **67**, 214508 (2003).

²⁵ O. Rösch, and O. Gunnarsson, *cond-mat/0308035*.

²⁶ A. V. Puchkov, P. Fournier, D. N. Basov, T. Timusk, A. Kapitulnik, and N. N. Kolesnikov, *Phys. Rev. Lett.* **77**, 3212 (1996), and D. N. Basov, R. Liang, B. Dabrowski, D. A. Bonn, W. N. Hardy, and T. Timusk, *Phys. Rev. Lett.* **77**, 4090 (1996).

²⁷ E. J. Singley, D. N. Basov, K. Kurahashi, T. Uefuji and K. Yamada, *Phys. Rev. B* **64**, 224503 (2003).

²⁸ X. J. Zhou, T. Yoshida, A. Lanzara, P. V. Bogdanov, S. A. Keller, K. M. Shen, W. L. Yang, F. Ronning, T. Sasagawa, T. Kakeshita, T. Noda, H. Eisaki, S. Uchida, C. T. Lin, F. Zhou, J. W. Xiang, W. X. Ti, Z. X. Zhao, A. Fujimori, Z. Hussain, and Z. -X. Shen, *Nature* **423**, 398 (2003).

²⁹ M. Eschrig, and M. R. Norman, *Phys. Rev. Lett.* **85**, 3261 (2000).

³⁰ D. Manske, I. Eremin, and K. H. Bennemann, *Phys. Rev. Lett.* **87**, 177055 (2003).

³¹ A. Lanzara, *et al.* (unpublished).

³² A. D. Gromko, A. V. Fedrov, Y. -D. Chuang, J. D. Korelek, Y. Aiura, Y. Yamaguchi, K. Oka, Y. Ando, and D. S. Dessau, *cond-mat/0202329*.

³³ T. Satoh, T. Takahashi, H. Ding, H. -B. Yang, S. -C. Wang, T. Fujii, T. Watanabe, A. Matsuda, T. Terashima, and K. Kadowaki, *Phys. Rev. Lett.* **91**, 157003 (2002).

³⁴ T. Cuk, F. Baumberger, D. H. Lu, N. Ingle, X. J. Zhou, H. Eisaki, N. Kaneko, Z. Hussain, N. Nagaosa, and Z. -X. Shen, (unpublished).

³⁵ I. Affleck, Z. Zou, T. Hsu, and P. W. Anderson, *Phys. Rev. B* **38**, 745 (1988).

³⁶ X. -G. Wen, and P. A. Lee, *Phys. Rev. Lett.* **76**, 503 (1996).

³⁷ P. A. Lee, N. Nagaosa, T. -K. Ng, and X. -G. Wen, *Phys. Rev. B* **57**, 6003 (1998).

³⁸ J. Brinckmann, and P. A. Lee, *Phys. Rev. B* **65**, 014502 (2001).

³⁹ P. A. Lee, and N. Nagaosa, *Phys. Rev. B* **68**, 024516 (2003).

⁴⁰ R. Zeyher, and M. L. Kulic, *Phys. Rev. B* **53**, 2850 (1996).

⁴¹ J. H. Kim, K. Levin, R. Wentzcovitch, and A. Auervach, *Phys. Rev. B* **44**, 5148 (1991).

⁴² F. C. Zhang, and T. M. Rice, *Phys. Rev. B* **37**, 3759 (1988).

⁴³ J. Lorenzana, and G. A. Sawatzky, *Phys. Rev. Lett.* **74**,

1876 (1995).

⁴⁴ M. R. Norman, M. Randeria, H. Ding, and J. C. Campuzano, Phys. Rev. B **52**, 615 (1995).

⁴⁵ Y. DeWilde, N. Miyakawa, P. Guptasarma, M. Iavarone, L. Ozyuzer, J. F. Zasadzinski, P. Romano, D. G. Hinks, C. Kendziora, G. W. Crabtree, and K. E. Gray, Phys. Rev. Lett. **80**, 153 (1998).

⁴⁶ Ch. Renner, B. Revaz, J. -Y. Genoud, K. Kadouaki, and Ø. Fischer, Phys. Rev. Lett. **80**, 149 (1998).

⁴⁷ W. Götze, and P. Wölfle, Phys. Rev. B **6**, 1226 (1972).

⁴⁸ H. Takagi, B. Batlogg, H. L. Kao, J. Kow, R. J. Cava, J. J. Krajewski, and W. F. Peck, Jr, Phys. Rev. Lett. **69**, 2975 (1992).

⁴⁹ P. V. Bogdanov, A. Lanzana, X. J. Zhou, W. L. Yang, H. Eisaki, Z. Hussain, and Z. -X. Shen, Phys. Rev. Lett. **89**, 167002 (2002).

⁵⁰ J. B. Marston, and I. Affleck, Phys. Rev. B **39**, 11 538 (1989).

⁵¹ N. Read, and E. Sachdev, Phys. Rev. Lett. **62**, 1694 (1989).

⁵² J. W. Loram, K. A. Mirza, J. M. Wade, J. R. Cooper, and W. Y. Liang, Physica C **235-240**, 134 (1994), and J. W. Loram, K. A. Mirza, J. R. Cooper, and J. L. Tallon, Physica C **282-287**, 1405 (1997).

⁵³ F. Ronning, C. Kim, D. L. Feng, D. S. Marshall, A. G. Loeser, L. L. Miller, J. N. Eckstein, I. Bozovic, and Z. -X. Shen, Science **282**, 2067 (1998).

⁵⁴ A. S. Mishchenko *et al.*, (unpublished).